Exceptional points in the Riesz-Feller Hamiltonian with an impenetrable rectangular potential

Michael Berman[1,*] and Nimrod Moiseyev[2,†]

[1]*Computer Science Department, Hadassah Academic College, 37 Hanevi'im Street, P.O. Box 1114, Jerusalem 9101001, Israel*

[2]*Schulich Faculty of Chemistry and Faculty of Physics Solid State Institute, Technion-Israel Institute of Technology, 32000 Haifa, Israel*

(Received 27 August 2018; published 8 October 2018)

The number of bound states in a standard rectangular potential well depends on the potential depth and width. In an impenetrable one-dimensional rectangular potential well, there are infinite bound states. In this work we study a non-Hermitian Riesz-Feller kinetic energy; i.e., the second-order derivative of the standard kinetic energy operator is replaced by a fractional, αth-order derivative. We show that for $\alpha < 2$ a particle in an impenetrable one-dimensional rectangular potential well contains a finite number of bound states and an infinite number of metastable decaying states. The transitions from bound states to metastable decaying states occur at α values that correspond to exceptional points, for which two bound states coalesce. Our findings indicate that one can describe a transition of highly excited bound states to metastable decaying states, for example due to the interactions of atoms and molecules with the environment, by using the Riesz-Feller kinetic energy operator rather than the standard one.

DOI: 10.1103/PhysRevA.98.042110

I. INTRODUCTION

The quantum well has important applications and theoretical value. In a quantum well semiconductor, a very thin layer of a small band gap material is sandwiched between two layers of a larger band gap material. Potential wells are established for electrons, at the top of the valence band and for the holes, at the bottom of the conduction band. Due to the electron and hole confinement in these potential wells and since the semiconductor dimension is comparable to the electron and hole de Broglie wavelength, energy levels of electrons and holes show very marked quantum-size effects. Semiconductor quantum wells, of either strained or unstrained type, have become the most widely used semiconductor-laser materials [1]. To calculate the energy levels of both electrons and holes in the corresponding quantum well, one uses the simplified assumption of infinite well depth. The Bloch wave functions, in both the conduction and valence bands, can then be written as eigenfunctions of the infinite square well. The improvement in optical properties obtained upon going from bulk material to the corresponding quantum well material is essentially due to a quantum confinement effect arising from the fact that one dimension of the semiconductor has become comparable to the de Broglie wavelength.

It was therefore natural to expand this idea to consider the other two possible cases of quantum confinement, namely, quantum wires and quantum dots (extremely small, on the scale of nanometers, semiconductors), where two or all three dimensions become comparable to the de Broglie wavelength [1]. Another application of a one-dimensional particle in a box is in conjugated polyene systems. The size of the box is taken equal to bond distance from one terminus of the polyene to the other [2].

The number of bound states in a rectangular potential well in quantum mechanics depends on the potential depth and width. In particular, if the potential well is finite, the number of bound states is finite and is accompanied by other kinds of states, such as antibound and metastable decaying states. At particular values of the parameters, exceptional points (EPs) are encountered [3,4]. Very near these exceptional points, bound states are transformed into antibound states. When inspecting gradually lower energies below some threshold energy, it was found [4] that two antibound states suddenly coalesce, resulting in capture resonances. These nonsmooth transitions are not typical to other potentials and were considered nonphysical.

In this work we show that with a non-Hermitian Riesz-Feller kinetic energy (i.e., with fractional derivative), the impenetrable one-dimensional rectangular potential well contains a finite number of bound states and an infinite number of metastable decaying states. More background and references on the Riesz-Feller derivative are in Sec. II A below. The problem to determine the eigenfunctions and eigenvalues of the one-dimensional time-independent fractional Schrödinger equation with the impenetrable one-dimensional rectangular potential well is intriguing and possibly still open [5]. In this work we solve this problem using the impenetrable one-dimensional rectangular potential well eigenfunctions as a basis set. By doing so, we assure the same boundary conditions for the fractional impenetrable one-dimensional rectangular potential well problem, i.e., that the wave functions vanish on the edges of the box. Matrix elements of the Riesz-Feller Hamiltonian are calculated with this basis set in closed form and the resulting matrix Hamiltonian is diagonalized numerically. We discover that the Riesz-Feller fractional impenetrable one-dimensional rectangular potential well possesses exceptional points. Exceptional points

*michael@hac.ac.il

†nimrod@technion.ac.il

are spectral singularities that occur generically in eigenvalue problems depending on a parameter [6–9]. Exceptional points are featured in quantum phase transitions and quantum chaos, and they produce dramatic effects in multichannel scattering, specific time dependence, and more. In nuclear physics they are associated with instabilities and affect approximation schemes. Exceptional points could be of interest for weakly bound states such as halos and nuclei along the drip line [10]. The special situation of exceptional points is associated with a branch point in the complex energy plane. With respect to the c-product defined for non-Hermitian operators (matrices), the degenerate eigenstate is self-orthogonal [7].

As a branch point in the spectrum is removed by any infinitesimally small external perturbation, it seems to be inaccessible experimentally and may be considered just as a mathematical object rather than a physical one. However, as shown in [11,12], varying the potential parameters reveals the existence of a branch point in time-independent as well as in time-dependent measurements of state exchanges in microwave experiments. Moreover, sufficiently close to the branch point, the eigenfunctions of the coalescing eigenvalues are nearly self-orthogonal [7]. By normalizing these nearly degenerate states to unity, the amplitudes of the wave function become enormously large sufficiently close to the exceptional point. In [13] the terminology "self-orthogonality" was first presented, in order to emphasize the coalescence of the eigenstates near exceptional points.

As reported in the results (Sec. III) of this paper, we observe all these effects near the exceptional points of the Riesz-Feller impenetrable one-dimensional rectangular potential well.

Indeed, in this work we show that at each exceptional point of the Riesz-Feller impenetrable one-dimensional rectangular potential well, the number of bound states is increased (decreased) by two, and thereby the number of metastable decaying states is decreased (increased) by two. At the exceptional point the highest two bound states are degenerate.

II. THEORY

A. Fractional calculus and the Riesz-Feller derivative

A recent historical survey [14] attributes the birth of fractional calculus to N. H. Abel. In his article [15] Abel introduced fractional order integration in the form that is currently known as the Riemann-Liouville fractional integral, and fractional-order differentiation in the form that is currently known as the Caputo fractional derivative. A comprehensive account of the field is covered in [16] with an early survey of applications in chapter 10 therein. Fractional calculus was shown to describe physical phenomena where conventional approaches have been unsatisfactory. Recent progress in the theory and mathematical aspects in the field of fractional calculus have appeared in a series of papers, a special issue of the *Journal of Fractional Calculus and Applied Analysis* [17]. The special issue contains both survey and research papers on special functions and integral transforms, both very valuable to the field of fractional calculus. Another collection of very recent papers encompasses most of the important areas of fractional calculus research and applications [18]. A comprehensive and thorough book on the subject can be found in [19] and the relevance to physics is covered in [20].

Definition of the Riesz-Feller fractional derivative

We use the following convention for the Fourier transform:

$$f(k) \equiv F\{f(x);k\} = \int_{-\infty}^{\infty} e^{ikx} f(x)dx, \quad k \in R, \tag{1}$$

and the inverse Fourier transform:

$$\begin{aligned} f(x) &\equiv F^{-1}\{f(k);x\} \\ &= \frac{1}{2\pi}\int_{-\infty}^{\infty} e^{-ikx} f(k)dk, \quad x \in R. \end{aligned} \tag{2}$$

For a sufficiently well-behaved function $f(x)$ the Riesz-Feller fractional derivative ${}_xD_\theta^\alpha$ is defined through [21]

$$F\left\{{}_xD_\theta^\alpha f(x);k\right\} = -\psi_\alpha^\theta(k) f(k), \tag{3}$$

where

$$\begin{aligned} \psi_\alpha^\theta(k) &= |k|^\alpha e^{i[\mathrm{sgn}(k)]\theta\pi/2}, \quad 0 < \alpha \leqslant 2, \\ &|\theta| \leqslant \min\{\alpha, 2-\alpha\}. \end{aligned} \tag{4}$$

We note further that

$$\begin{aligned} {}_xD_\theta^\alpha f(x) &= F^{-1}\{F\{{}_{x'}D_\theta^\alpha f(x');k\},x\} \\ &= -\frac{1}{2\pi}\int_{-\infty}^{\infty} dk e^{-ikx}\psi_\alpha^\theta(k)\int_{-\infty}^{\infty} e^{ikx'} f(x')dx'. \end{aligned} \tag{5}$$

The allowed region for the parameters α and θ turns out to be a diamond in the plane $\{\alpha,\theta\}$ with vertices in the points (0, 0), (1, 1), (1, −1), (2, 0) that are called the *Feller-Takayasu diamond* [22]. Thus, one recognizes that the Riesz-Feller derivative is a pseudo-differential operator whose symbol $\psi_\alpha^\theta(k)$ is the logarithm of the characteristic function of a general Lévy strictly stable probability density with index of stability α and asymmetry parameter θ (also called *skewness*). The values that the index of stability and the asymmetry parameter can take on have been studied by Takayasu; see the Feller-Takaysu diamond diagram below:

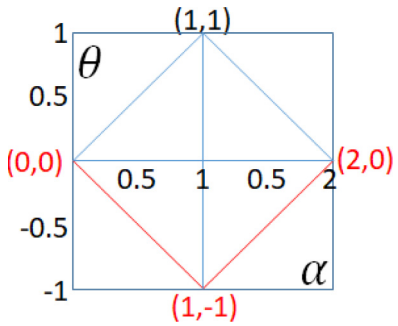

Feller-Takayasu diamond.

We note the following particular cases of the Riesz-Feller derivative, namely the standard derivatives, $\alpha = 2$ and $\alpha = 1$:

$$\begin{aligned} F\left\{{}_xD_0^2 f(x);k\right\} &= -\psi_2^0(k) f(k) = -|k|^2 f(k) \\ &= -k^2 f(k), \end{aligned} \tag{6}$$

consistent with $[F\{\frac{d^n}{dx^n}f(x);k\} = (ik)^n f(k)]_{n=2}$,

$$\begin{aligned} F\left\{{}_x D_{-1}^{1} f(x);k\right\} &= -\psi_1^{-1}(k) f(k) = -|k| e^{-i[\mathrm{sgn}(k)]\pi/2} f(k) \\ &= -|k|\{\cos[-(\mathrm{sgn}\, k)\pi/2] \\ &\quad + i\,\sin[-(\mathrm{sgn}\, k)\pi/2]\} f(k) \\ &= ikf(k), \end{aligned} \tag{7}$$

consistent with $[F\{\frac{d^n}{dx^n}f(x);k\} = (ik)^n f(k)]_{n=1}$.

Finally, for the special case $\theta = 0$, the Riesz-Feller derivative reduces to the Riesz derivative. Laskin [23] showed the Hermiticity of the fractional Hamilton operator based on the Riesz derivative. As we confirm in this work the Hamiltonian operator based on the Riesz-Feller derivative is non-Hermitian, apart from the special cases $\theta = 0$ (the Riesz derivative) and $\alpha = 2$ (the standard second-order derivative). We remark that in this paper we use Eq. (3) as the definition of the Riesz-Feller derivative, and therefore the Riesz derivative too. A different definition of the Riesz derivative through a principal value integral exists in the literature [19]. The two definitions are equivalent in cases where the argument of the Fourier transform is infinitely differentiable (belongs to a Schwartz space), which is not the case for the impenetrable one-dimensional rectangular potential well. This nonequivalence may be one of the origins of the debate, see [24–26] and references therein, regarding the form of the eigenvalues and eigenfunctions of the fractional impenetrable one-dimensional rectangular potential well with the Riesz derivative. Other aspects of the debate relate to the influence of using local versus nonlocal boundary conditions. Further considerations regarding this debate are beyond the scope of this paper.

B. The Riesz-Feller impenetrable one-dimensional rectangular potential well

1. Standard square well basis functions

As mentioned in Sec. I, we handle the Riesz-Feller impenetrable one-dimensional rectangular potential well problem using the complete basis set of the standard square well potential, namely via the eigenvalues and eigenfunctions, see Appendix A,

$$\langle x|\lambda_n\rangle = C\sin(\lambda_n x), \quad \lambda_n = \frac{n\pi}{a}, \quad C = \frac{\sqrt{2}}{\sqrt{a}}. \tag{8}$$

These functions form a complete orthonormal basis set on the interval $[0, a]$, with the inner product reviewed in Appendix A,

$$\langle\lambda_{n'}|\lambda_n\rangle = \int_0^a dx\,\langle\lambda_n|x\rangle\langle x|\lambda_n\rangle = \delta_{n',n}. \tag{9}$$

2. Impenetrable one-dimensional rectangular potential well with Riesz-Feller fractional derivative

We calculate matrix elements $\langle\lambda_{n'}|H_\alpha|\lambda_n\rangle$ of the following fractional Hamiltonian:

$$H_\alpha = -F_\alpha D_\theta^\alpha + V(x), \tag{10}$$

$$V(x) = \begin{cases} \infty, & x < 0, \\ 0, & 0 \leqslant x \leqslant a, \\ \infty, & x > a, \end{cases} \tag{11}$$

where F_α is the "quantum diffusion constant" with units of [ergs$^{1-\alpha}$ cm$^\alpha$ sec$^{-\alpha}$], and D_θ^α is the Riesz-Feller derivative defined above in Eq. (5). $F_\alpha := -\frac{1}{2}mc^2(\frac{\hbar}{imc})^\alpha$ [27], Eq. (14.11) therein, where m is the "mass" and c is the speed of light. Using the above square well basis functions of Eq. (8) ensures boundary conditions in which the wave functions (eigenfunctions of the fractional hamiltonian H_α) vanish at $x = 0$ and $x = a$, just as those of the standard impenetrable one-dimensional rectangular potential well. The problem of fractional differential equations, such as fractional diffusion, on bounded domains is nontrivial and was studied for example in [28,29] and references therein.

The closed form matrix elements in the $\langle x|\lambda_n\rangle$ basis, as obtained in Appendix B, Eq. (B14), are

$$\langle\lambda_{n'}|H_\alpha|\lambda_n\rangle = B_\alpha(n\pi)^\alpha \times \begin{cases} \sin\left(\theta\frac{\pi}{2}\right)\frac{2}{\pi}\left\{\frac{1}{(n'+n)} + \frac{1}{(n'-n)}\right\}; & n' \neq n,\ n'+n = \text{odd}; \\ 0; & n' \neq n,\ n'+n = \text{even}; \\ \cos\left(\theta\frac{\pi}{2}\right); & n' = n; \end{cases} \tag{12}$$

where

$$B_\alpha = \left(\frac{1}{a}\right)^\alpha F_\alpha, \qquad F_\alpha = -\frac{1}{2}mc^2\left(\frac{\hbar}{imc}\right)^\alpha. \tag{13}$$

Clearly, the Riesz Hamiltonian, namely the case $\theta = 0$, is diagonal in this basis and obviously Hermitian. Non-Hermitian behavior is caused by the asymmetry parameter $\theta \neq 0$ of the Lévy strictly stable probability density. It is instructive to analyze the units of B_α, namely, B_α in cgs:

$$\begin{aligned} &\left[\text{g cm}^2\ \text{s}^{-2}\left(\frac{\text{g cm}^2\ \text{s}^{-1}}{\text{g cm s}^{-1}}\right)^\alpha\right]\frac{1}{\text{cm}^\alpha} = [\text{g cm}^2\ \text{s}^{-2}(\text{cm})^\alpha]\frac{1}{\text{cm}^\alpha} \\ &= [\text{g cm}^2\text{s}^{-2}] = [\text{ergs}], \end{aligned} \tag{14}$$

B_α in atomic units:

$$\begin{aligned} &\left[m_e\text{bohrs}^{2+\alpha}\left(\frac{\hbar}{\text{hartrees}}\right)^{-2}\right]\frac{1}{\text{bohrs}^\alpha} \\ &= \left[m_e\text{bohrs}^2\left(\frac{\hbar}{\text{hartrees}}\right)^{-2}\right] \\ &= [\text{hartrees}]. \end{aligned} \tag{15}$$

In atomic units $\hbar = 1, m$ is expressed in multiples of the electron mass $m_e = 1$, and the speed of light $c \approx 137$.

B_α and $\langle\lambda_{n'}|H_\alpha|\lambda_n\rangle$ possess energy units, so that $\langle\lambda_{n'}|H_\alpha|\lambda_n\rangle/B_\alpha$ is a real nonsymmetric matrix with dimensionless units.

In [30], it was claimed that as the Hamiltonian with the Riesz-Feller derivative is non-Hermitian, it is not suitable for describing physical problems. As mentioned above, this is also the outcome of the present calculation; i.e., the Hamiltonian H_α is non-Hermitian. However, this does not mean

nonphysical, as is emphasized for example in the seminal review in Ref. [31] and in other recent publications [32,33].

The Feynman path integral approach to quantum mechanics [34] utilizes integration over Brownian-like quantum mechanical paths. The Brownian motion is a special case of the Lévy-stable random process, which corresponds to the Riesz-Feller derivative defined in Eq. (3). The above model may serve to describe one-dimensional integration over Lévy-like quantum mechanical paths of a particle in a box.

C. Exceptional points

As mentioned in the introduction, exceptional points (EPs) are featured in quantum phase transitions and quantum chaos, and they produce dramatic effects in multichannel scattering, specific time dependence, and more. In physics they are associated with instabilities and affect approximation schemes [7,8]. Let us denote the eigenvalues of $\langle\lambda_{n'}|H_\alpha|\lambda_n\rangle$ in Eq. (12) by E_α and $E_{\alpha_{\rm EP}}$ at the EP. As we show in the results section, Sec. III, EPs occur when one gradually increases the value of α in the range $0 < \alpha \leqslant 2$. At each EP, the two highest eigenvalues are degenerate. Furthermore, as the value of α is increased, more purely real eigenvalues occur, approaching infinitely many for $\alpha \to 2$, as it should for the standard impenetrable one-dimensional rectangular potential well. We expand E_α around $E_{\alpha_{\rm EP}}$ to calculate the following approximation:

$$E_\alpha \approx E_{\alpha_{\rm EP}} + a_1\sqrt{\alpha-\alpha_{\rm EP}} + a_2(\sqrt{\alpha-\alpha_{\rm EP}})^2 + a_3(\sqrt{\alpha-\alpha_{\rm EP}})^3 + a_4(\sqrt{\alpha-\alpha_{\rm EP}})^4. \tag{16}$$

In Eq. (16) the unknowns are a_1, a_2, a_3, a_4. We denote the known values in the above square root expressions by $y_i := \sqrt{\alpha_i - \alpha_{\rm EP}}$, $i = 1, 2, 3, 4$, and the corresponding exact eigenvalues by E_{α_i}, $i = 1, 2, 3, 4$ (taken to be known in this context) and then collect the latter in a known vector E and the unknowns in a vector A, namely in

$$E = \begin{pmatrix} E_{\alpha_1} \\ E_{\alpha_2} \\ E_{\alpha_3} \\ E_{\alpha_4} \end{pmatrix}, \quad E_{\rm EP} = \begin{pmatrix} E_{\alpha_{\rm EP}} \\ E_{\alpha_{\rm EP}} \\ E_{\alpha_{\rm EP}} \\ E_{\alpha_{\rm EP}} \end{pmatrix}, \quad A = \begin{pmatrix} a_1 \\ a_2 \\ a_3 \\ a_4 \end{pmatrix}. \tag{17}$$

Using Eq. (16), we obtain the following four equations:

$$\begin{aligned} E_{\alpha_1} &\approx E_{\alpha_{\rm EP}} + a_1 y_1 + a_2 y_1^2 + a_3 y_1^3 + a_4 y_1^4, \\ E_{\alpha_2} &\approx E_{\alpha_{\rm EP}} + a_1 y_2 + a_2 y_2^2 + a_3 y_2^3 + a_4 y_2^4, \\ E_{\alpha_3} &\approx E_{\alpha_{\rm EP}} + a_1 y_3 + a_2 y_3^2 + a_3 y_3^3 + a_4 y_3^4, \\ E_{\alpha_4} &\approx E_{\alpha_{\rm EP}} + a_1 y_4 + a_2 y_4^2 + a_3 y_4^3 + a_4 y_4^4. \end{aligned} \tag{18}$$

We further define the matrix

$$Y = \begin{pmatrix} y_1 & y_1^2 & y_1^3 & y_1^4 \\ y_2 & y_2^2 & y_2^3 & y_2^4 \\ y_3 & y_3^2 & y_3^3 & y_3^4 \\ y_4 & y_4^2 & y_4^3 & y_4^4 \end{pmatrix} \tag{19}$$

to cast Eq. (18) in matrix form as

$$E - E_{\rm EP} \approx YA. \tag{20}$$

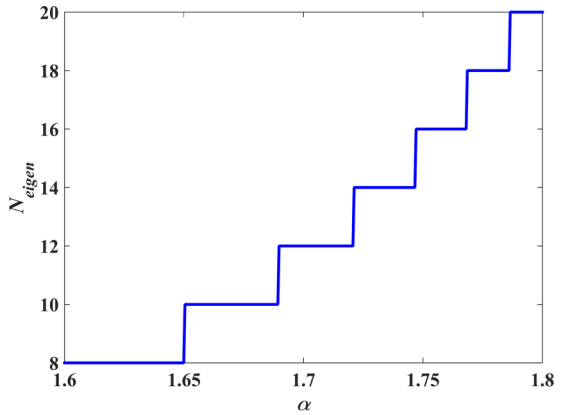

FIG. 1. $N_{\rm eigen}$, the number of real eigenvalues, is shown as a function of the fractional derivative order α. At the limit $\alpha \to 2$, the number of bound states goes to infinity, i.e., $N_{\rm eigen} \to \infty$. The jumps take place when the two largest real eigenvalues become degenerate. These degeneracies of the non-Hermitian Hamiltonian when α is not equal to an integer are exceptional points, EPs, in the spectrum. As we show later, the corresponding degenerate eigenfunctions coalesce and the number of linearly independent eigenfunctions and eigenvectors is smaller than the dimension of the Hamiltonian matrix constructed with the square well basis functions. Here the number of square well basis functions is 250, and the size of the square well box $a = 1$. The number of real eigenvalues is even for an even number of basis functions and odd for an odd number of basis functions.

Therefore, the unknown vector A is obtained from

$$A \approx Y^{-1}(E - E_{\rm EP}). \tag{21}$$

Equation (16) is used in the results section, Sec. III, with the calculated values of the elements of the matrix A in Eq. (21) to approximate the eigenvalues near the EPs, and then these approximate values are compared to the exact eigenvalues of $\langle\lambda_{n'}|H_\alpha|\lambda_n\rangle$ in Eq. (12).

III. RESULTS

In this section we investigate the properties of the *Riesz-Feller* impenetrable one-dimensional rectangular potential problem using the closed form Eq. (12) for the non-Hermitian Hamiltonian matrix $\langle\lambda_{n'}|H_\alpha|\lambda_n\rangle$. We calculate numerically the dimensionless eigenvalues E_α/B_α, and the left and right eigenfunctions of this matrix, $\langle\psi_\alpha^L|x\rangle$ and $\langle x|\psi_\alpha^R\rangle$, respectively. In the series of Figs. 1–8, we demonstrate the properties of these eigenvalues and eigenfunctions. In particular, we show the existence of a finite number of purely real eigenvalues, in contradistinction to the classical impenetrable one-dimensional rectangular potential well with the integer derivative in the kinetic energy term, for which there is an infinite number of real eigenvalues. We show the dependence of these eigenvalues and eigenfunctions on the value of the fractional order α of the derivative in the kinetic energy term. For gradually increased values of α, in the range $0 < \alpha \leqslant 2$, more eigenvalues become real. Furthermore, we prove the existence of exceptional points (EP) at particular values of $\alpha = \alpha_{\rm EP}$. The number of real eigenvalues is abruptly increased by two at each EP. It is shown that at the EP the highest two real eigenvalues are degenerate, resulting in enhancements of

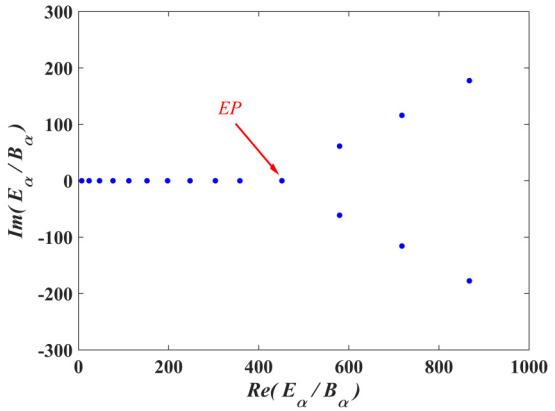

FIG. 2. Imaginary part of low-lying eigenvalues, $\mathrm{Im}(E_\alpha/B_\alpha)$ in dimensionless units, as a function of the real part of these eigenvalues, $\mathrm{Re}(E_\alpha/B_\alpha)$ in dimensionless units, for $\alpha = \alpha_{\mathrm{EP}} = 1.68961520687$. For this value of α there are 12 real eigenvalues, the highest two of which are degenerate, at the exceptional point. The red arrow points to the exceptional point (EP). The number of square well basis functions is 250, and the size of the square well box $a = 1$.

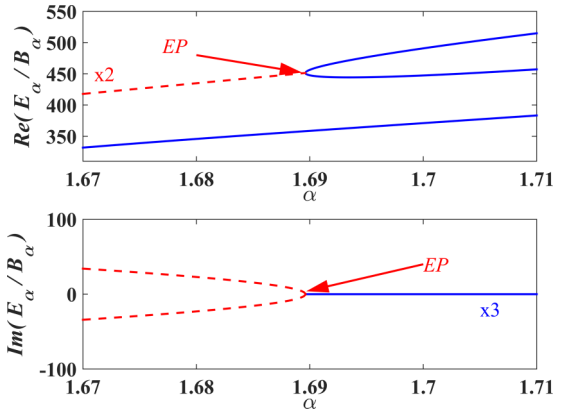

FIG. 3. Largest 3 real eigenvalues, $\mathrm{Re}(E_\alpha/B_\alpha)$ in dimensionless units, in blue (dimensionless units) for each α. At $\alpha = \alpha_{\mathrm{EP}} = 1.68961520687$ the eigenvalues are degenerate, i.e., an exceptional point (EP) indicated by the red arrow. The red dashed lines indicate the two complex eigenvalues above the largest real eigenvalue; as can be seen, they possess the same real part in the α range below the exceptional point. The number of real eigenvalues increases by 2 when increasing α just above α_{EP}. The number of square well basis functions $N = 250$, and the size of the square well box $a = 1$.

the value of the eigenfunction amplitudes. The consequences of this enhancement are discussed later in the discussion section. In passing, the accuracy of the algebraic expansion near the EP, Eq. (16), is studied.

The number of real eigenvalues N_{eigen} is dependent on the value of the fractional derivative order α as shown in Fig. 1. Jumps in this number take place for values of the derivative order α for which the two largest real eigenvalues become degenerate. These degeneracies of the non-Hermitian Hamiltonian matrix $\langle\lambda_{n'}|H_\alpha|\lambda_n\rangle$ in Eq. (12), when α is not equal to an integer, are typical for exceptional points (EPs) in the spectrum. As we show later, the corresponding degenerate eigenfunctions coalesce and the number of linearly independent eigenfunctions and eigenvectors is smaller than the dimension of the Hamiltonian matrix constructed with the square well basis functions.

The appearance of an exceptional point is apparent when displaying the imaginary part $\mathrm{Im}(E_\alpha/B_\alpha)$ as a function of the real part $\mathrm{Re}(E_\alpha/B_\alpha)$, both in dimensionless units, obtained from the diagonalization of $\langle\lambda_{n'}|H_\alpha|\lambda_n\rangle/B_\alpha$ of Eq. (12) [with B_α of Eq. (13)]. This is shown in Fig. 2 at an exceptional point value of $\alpha = \alpha_{\mathrm{EP}} = 1.68961520687$. For this value of α there are 12 real eigenvalues, of which the highest two are degenerate. The arrow in Fig. 2 points to the exceptional point degenerate eigenvalues. The eigenvalues to the left of this point are real (12 bound states for this value of α_{EP}) and to the right of this point they are complex (metastable decaying states). The infinite number of metastable decaying states occur in complex conjugate pairs. Only three of the metastable decaying state eigenvalues are displayed in Fig. 2.

It is instructive to inspect the largest eigenvalues as a function of the derivative order α. In Fig. 3, the largest three real eigenvalues are shown with a full line for each α. At $\alpha = \alpha_{\mathrm{EP}} = 1.68961520687$ the eigenvalues are real and degenerate; i.e., this is an exceptional point indicated by the arrow. The dashed lines indicate the two complex eigenvalues just above the largest real eigenvalue. As can be seen, they possess the same real part in the α range below the EP and the imaginary parts coalesce to zero above the EP. Clearly, the number of real eigenvalues increases by 2 when increasing α just above α_{EP} as was shown also in Fig. 1.

The eigenfunctions of the Riesz-Feller impenetrable one-dimensional rectangular potential well can be calculated with the eigenvectors of the the matrix $\langle\lambda_{n'}|H_\alpha|\lambda_n\rangle/B_\alpha$ of Eq. (12), In Fig. 4, the top panels display the right eigenfunctions $\psi^R(x)$ corresponding to the 12th real eigenvalue of this matrix $\langle\lambda_{n'}|H_\alpha|\lambda_n\rangle/B_\alpha$, and the middle panels display the left eigenfunctions $\psi^L(x)$ corresponding to the 12th real eigenvalue (using the right eigenvector of the transposed matrix). The bottom panels display the products $\rho(x) = \psi^L(x)\psi^R(x)$ of these eigenfunctions. The left-hand bottom panel, $\alpha = \alpha_{\mathrm{EP}} = 1.68961520687$, displays the exceptional point product $\psi^L_{\mathrm{EP}}(x)\psi^R_{\mathrm{EP}}(x)$, for which the left and right eigenvectors of the matrix are orthogonal, i.e., the matrix element $\langle\psi^L_{\alpha_{\mathrm{EP}}}|\psi^R_{\alpha_{\mathrm{EP}}}\rangle = 2.80111 \times 10^{-08}$, and therefore is non-normalizable. The center bottom panel displays the product $\psi^L(x)\psi^R(x)$, for which $\langle\psi^L(x)|\psi^R(x)\rangle = 0.0011524$, nonzero and normalizable. The right-hand bottom panel, $\alpha = 2$, displays the product $\psi^L(x)\psi^R(x)$ for which $\langle\psi^L(x)|\psi^R(x)\rangle = 1$, also of course nonzero and normalizable. Note that the eigenfunctions are far from being trigonometric in their functional form except for $\alpha = 2$.

As mentioned earlier, the left and right eigenfunctions, $\psi^L(x)$, $\psi^R(x)$, respectively, are self-orthogonal at the exceptional point. This feature is demonstrated in Fig. 5, where the matrix element $\langle\psi^L(x)|\psi^R(x)\rangle$ is shown as a function of α. At the exceptional point $\alpha_{\mathrm{EP}} = 1.68961520687$, the product $\langle\psi^L_{\alpha_{\mathrm{EP}}}|\psi^R_{\alpha_{\mathrm{EP}}}\rangle \cong 0$ meaning that ψ^L_{EP} and ψ^R_{EP} are orthogonal and the corresponding eigenvalues are degenerate. The two linearly independent solutions are $(\psi^L_{\alpha_{\mathrm{EP}}}, \psi^R_{\alpha_{\mathrm{EP}}})$ and $(i\psi^L_{\alpha_{\mathrm{EP}}}, i\psi^R_{\alpha_{\mathrm{EP}}})$. The left and right eigenfunctions are obtained

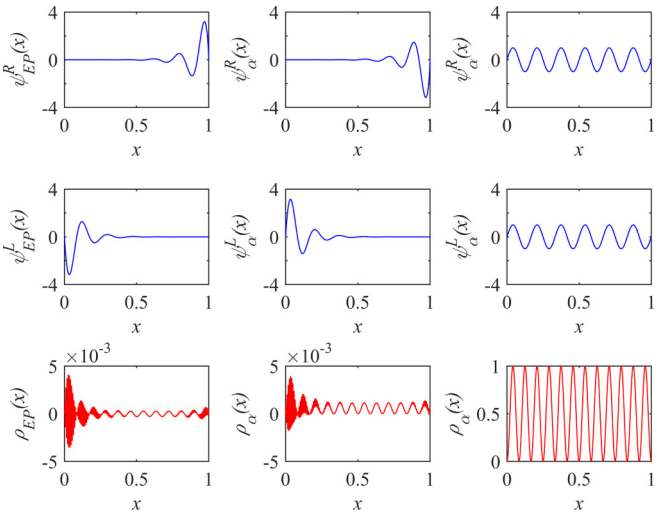

FIG. 4. The top panels display the right eigenfunctions $\psi^R(x)$ corresponding to the 12th real eigenvalue of the matrix, and the middle panels display the left eigenfunctions $\psi^L(x)$ corresponding to the 12th real eigenvalue (right eigenvalue of the transposed matrix). The bottom panels display the products $\rho(x) = \psi^L(x)\psi^R(x)$. The left-hand bottom panel, $\alpha = \alpha_{\rm EP} = 1.68961520687$, displays the product $\psi^L_{\rm EP}(x)\psi^R_{\rm EP}(x)$, for which the left and right eigenvectors of the matrix are orthogonal, i.e., the matrix element $\langle\psi^L_{\alpha_{\rm EP}}|\psi^R_{\alpha_{\rm EP}}\rangle = 2.80111 \times 10^{-08}$ and therefore is non-normalizable. The center bottom panel displays the product $\psi^L(x)\psi^R(x)$ for which $\langle\psi^L(x)|\psi^R(x)\rangle = 0.0011524$, nonzero and normalizable. The right-hand bottom panel, $\alpha = 2$, displays the product $\psi^L(x)\psi^R(x)$ for which $\langle\psi^L(x)|\psi^R(x)\rangle = 1$, also of course nonzero and normalizable. Note that the eigenfunctions are far from being trigonometric in their functional form except for $\alpha = 2$. The number of square well basis functions $N = 250$, and the size of the square well box $a = 1$.

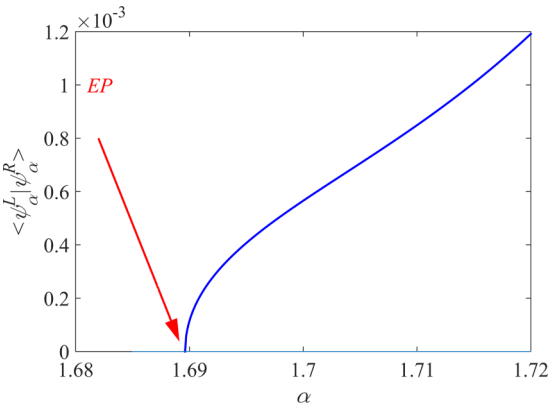

FIG. 5. The matrix element $\langle\psi^L(x)|\psi^R(x)\rangle$ as a function of α. At the exceptional point (EP) $\alpha_{\rm EP} = 1.68961520687$, the product $\langle\psi^L_{\alpha_{\rm EP}}|\psi^R_{\alpha_{\rm EP}}\rangle \cong 0$ meaning that $\psi^L_{\rm EP}$ and $\psi^R_{\rm EP}$ are orthogonal and the corresponding eigenvalues are degenerate. The two linearly independent solutions are $(\psi^L_{\alpha_{\rm EP}}, \psi^R_{\alpha_{\rm EP}})$ and $(i\psi^L_{\alpha_{\rm EP}}, i\psi^R_{\alpha_{\rm EP}})$. The left and right eigenfunctions are obtained by expanding them in the particle-in-a-box basis functions where the corresponding coefficients are respectively obtained from the diagonalization of the Hamiltonian matrix and its transpose. Here the number of square well basis functions $N = 250$, and the size of the square well box $a = 1$.

by expanding them in the particle-in-a-box basis functions where the corresponding coefficients are respectively obtained from the diagonalization of the Hamiltonian matrix $\langle\lambda_{n'}|H_\alpha|\lambda_n\rangle/B_\alpha$ of Eq. (12) and its transpose.

In Sec. II C an approximate formula for the eigenvalues near an exceptional point was suggested. This approximation is demonstrated in Fig. 6, where the largest two real eigenvalues are displayed as a function of α with a thick line. The approximate calculation for the highest eigenvalue using the algebraic expansion of Eq. (16) is displayed in dashed curves. The thin dashed (red) line is with one term in the expansion, i.e., up to order $\sqrt{\alpha - \alpha_{\rm EP}}$ in Eq. (16). The thick dashed (white) line is the calculated eigenvalue with the four terms of Eq. (16), i.e., up to order $(\sqrt{\alpha - \alpha_{\rm EP}})^4$. As can be seen, the latter approximation coincides with the exact largest real eigenvalue.

For the purpose of demonstrating the behavior and effects of exceptional points, it is instructive to inspect the ratio $P_\alpha = |\langle\psi^L(x)|\psi^L(x)\rangle\langle\psi^R(x)|\psi^R(x)\rangle/\langle\psi^L(x)|\psi^R(x)\rangle|^2$ as a function of α. This is demonstrated in Fig. 7, where the logarithm of the ratio P_α is shown as a function of α. We note that in our case the individual states are chosen normalized to unity, i.e., $\langle\psi^L(x)|\psi^L(x)\rangle = 1$ and $\langle\psi^R(x)|\psi^R(x)\rangle = 1$. At the exceptional point $\alpha = \alpha_{\rm EP} = 1.68961520687$, the ratio P_α diverges, which is a consequence of the non-normalizable product $\langle\psi^L_{\alpha_{\rm EP}}|\psi^R_{\alpha_{\rm EP}}\rangle$. As done in the previous figure, the left and right eigenfunctions are obtained by expanding them in the particle-in-a-box basis functions where the corresponding coefficients are obtained from the diagonalization of the Hamiltonian matrix $\langle\lambda_{n'}|H_\alpha|\lambda_n\rangle/B_\alpha$ of Eq. (12) and its transpose.

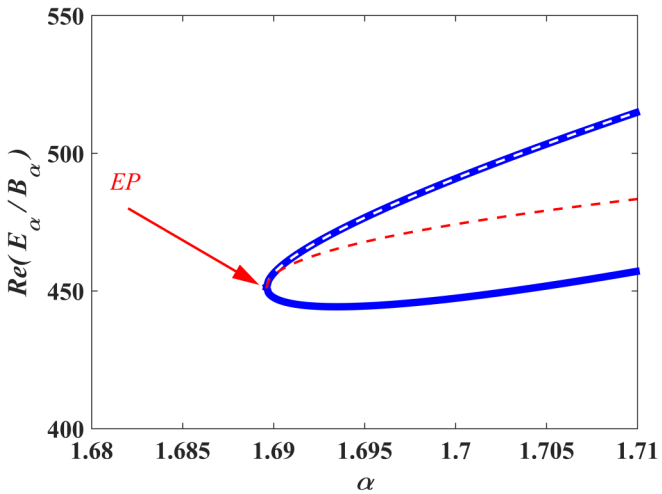

FIG. 6. Largest two real eigenvalues, $\mathrm{Re}(E_\alpha/B_\alpha)$ in dimensionless units, as a function of α displayed with a thick blue line. The approximate calculation for the highest eigenvalue using an algebraic expansion is displayed in dashed white and dashed red curves. The dashed red line is with one term in the expansion, i.e., up to order $\sqrt{\alpha - \alpha_{\rm EP}}$. The dashed white line is the calculated eigenvalue with four terms, i.e., up to order $(\sqrt{\alpha - \alpha_{\rm EP}})^4$. The latter coincides with the largest real eigenvalue. The number of square well basis functions $N = 250$, and the size of the square well box $a = 1$.

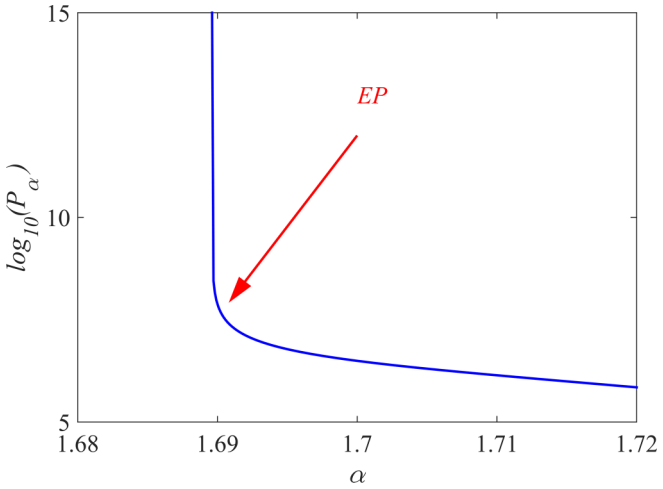

FIG. 7. The logarithm of the ratio $P_\alpha = |\langle\psi^L(x)|\psi^L(x)\rangle\langle\psi^R(x)|\psi^R(x)\rangle/\langle\psi^L(x)|\psi^R(x)\rangle|^2$ as a function of α. We note that in our case the individual states are chosen normalized to unity, i.e., $\langle\psi^L(x)|\psi^L(x)\rangle = 1$ and $\langle\psi^R(x)|\psi^R(x)\rangle = 1$. At the exceptional point (EP) $\alpha = \alpha_{\rm EP} = 1.68961520687$, the ratio P_α diverges, which is a consequence of the non-normalizable product $\langle\psi^L_{\alpha_{\rm EP}}|\psi^R_{\alpha_{\rm EP}}\rangle$. The left and right eigenfunctions are obtained by expanding them in the particle-in-a-box basis functions where the corresponding coefficients are respectively obtained from the diagonalization of the Hamiltonian matrix and its transpose. Here the number of square well basis functions $N = 250$, and the size of the square well box $a = 1$.

Finally, for the sake of further demonstrating the appearance and behavior of exceptional points, we collect in Fig. 8 the separate real and imaginary values of the first 10 eigenvalues and show them as a function of α. The top panel shows that for each eigenvalue, there is a large enough value of α, in which the real value splits, reflecting a transition from complex eigenvalues (where one is a complex conjugate of the other one) into two distinct real eigenvalues. The splitting takes place at the exceptional point. The bottom panel shows the imaginary part of the eigenvalues as a function of α, showing the fact that the eigenvalues are complex conjugates of each other and that from a large enough value of α (the EP point), the imaginary part vanishes.

IV. DISCUSSION AND CONCLUDING REMARKS

In this work we showed that with a non-Hermitian Riesz-Feller kinetic energy, the impenetrable one-dimensional rectangular potential well problem contains a finite number of bound states and an infinite number of metastable decaying states. Exceptional points for the Riesz-Feller impenetrable one-dimensional rectangular potential well problem are identified. Furthermore, we show physically viable abrupt transitions from bound states into metastable decaying states as the order α of the Riesz-Feller derivative is changed. These exceptional points are a consequence of the non-Hermitian nature of the Hamiltonian H_α.

We further mention that this non-Hermitian feature results when the asymmetry parameter θ of the Riesz-Feller

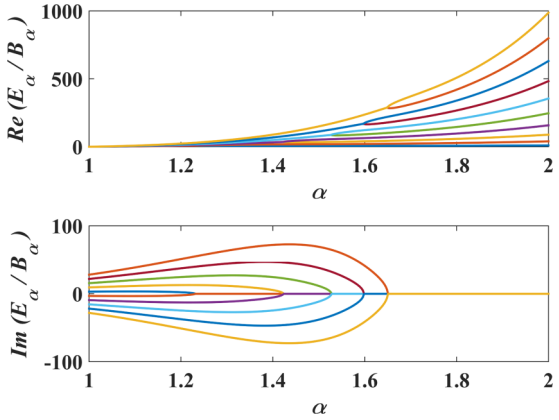

FIG. 8. The real and imaginary values of the first 10 eigenvalues as a function of α. The top panel shows that for each eigenvalue, there is a large enough value of α, in which the real value splits, reflecting a transition from complex eigenvalues (where one is a complex conjugate of the other one) into two distinct real eigenvalues. The splitting takes place at the EP. The bottom panel shows the imaginary part of the eigenvalues as a function of α, showing the fact that the eigenvalues are complex conjugates of each other and that from a large enough value of α (the EP point), the imaginary part vanishes. The number of square well basis functions $N = 250$, and the size of the square well box $a = 1$.

derivative is nonzero. Such asymmetry should be measurable in applications such as the semiconductor-laser materials and the conjugated polyene systems mentioned in the introduction. Our findings show that one can describe a transition of highly excited bound states of atoms or molecules to metastable decaying states, as occur for example due to the interactions with the environment, by using the Riesz-Feller kinetic energy operator rather than the standard one. We believe that our approach might open new directions of research where interaction of bound systems with the environment can be taken into consideration. Such applications of our method are phenomenological, in the same manner as are other approaches, such as the Lindblad approach [35–37].

APPENDIX A: THE STANDARD SQUARE WELL

The Schrödinger equation for the standard nonsymmetric square well is

$$H = -\frac{\hbar^2}{2m}\frac{\partial^2}{\partial x^2} + V(x), \tag{A1}$$

$$V(x) = \begin{cases} \infty, & x < 0, \\ 0, & 0 \leqslant x \leqslant a, \\ \infty, & x > a. \end{cases} \tag{A2}$$

The well-known eigenvalues and eigenfunctions of this Hamiltonian are

$$\langle\lambda_{n'}|H|\lambda_n\rangle = \frac{h^2}{8ma^2}n^2\delta_{n',n}, \tag{A3}$$

$$\langle x|\lambda_n\rangle = C\sin(\lambda_n x), \quad \lambda_n = \frac{n\pi}{a}, \quad C = \frac{\sqrt{2}}{\sqrt{a}}. \tag{A4}$$

These eigenfunctions form a complete orthonormal set. For completeness we review the orthonormality as follows:

$$\begin{aligned}\langle\lambda_{n'}|\lambda_n\rangle &= \int_0^a dx\,\langle\lambda_{n'}|x\rangle\langle x|\lambda_n\rangle \\ &= \int_0^a dx\; C\sin(\lambda_{n'}x)C\sin(\lambda_n x).\end{aligned} \tag{A5}$$

This integral is calculated via the following identities:

$$\sin(\lambda_n x) = \sin\left(\frac{n\pi}{a}x\right), \tag{A6}$$

$$C\sin\left(\frac{n'\pi}{a}x\right)C\sin\left(\frac{n\pi}{a}x\right) = C^2 \times \begin{cases}\frac{1}{2}[\cos(\frac{n'\pi}{a}x-\frac{n\pi}{a}x)-\cos(\frac{n'\pi}{a}x+\frac{n\pi}{a}x)], & n'\neq n,\\ \frac{1}{2}[1-\cos(2\frac{n\pi}{a}x)], & n'=n.\end{cases} \tag{A7}$$

Therefore, the integral in Eq. (A5) is

$$\int_0^a dx\; C\sin\left(\frac{n'\pi}{a}x\right)C\sin\left(\frac{n\pi}{a}x\right) = C^2 \times \begin{cases}\frac{a}{2}[\frac{\sin(n'\pi-n\pi)}{n'\pi-n\pi}-\frac{\sin(n'\pi+n\pi)}{n'\pi+n\pi}], & n'\neq n,\\ \frac{1}{2}[a-\sin(2n\pi)], & n'=n,\end{cases} \tag{A8}$$

or, as $\sin(n\pi)=0$ for all n, Eq. (A5) becomes

$$\langle\lambda_{n'}|\lambda_n\rangle = \int_0^a dx C\sin\left(\frac{n'\pi}{a}x\right)C\sin\left(\frac{n\pi}{a}x\right) = \frac{2}{a} \times \begin{cases}0, & n'\neq n\\ \frac{a}{2}, & n'=n\end{cases} = \delta_{n',n}. \tag{A9}$$

The resolution of the identity operator $\hat{I}$ (completeness of the eigenfunctions set) reads

$$\hat{I} = \sum_{i=1}^{\infty}|\lambda_i\rangle\langle\lambda_i|. \tag{A10}$$

APPENDIX B: THE FRACTIONAL SQUARE WELL

1. The Riesz-Feller derivative with the momentum variable

We now move to using the momentum p, through $k = p/\hbar$. The Fourier transform and its inverse, Eqs. (1) and (2), respectively take the form

$$\begin{aligned}f(p/\hbar) &\equiv F\{f(x);p/\hbar\} \\ &= \int_{-\infty}^{\infty} e^{i\frac{p}{\hbar}x}f(x)dx, \qquad p/\hbar\in R,\end{aligned} \tag{B1}$$

$$\begin{aligned}F^{-1}\{f(p/\hbar);x\} &= \frac{1}{2\pi\hbar}\int_{-\infty}^{\infty} e^{-i\frac{p}{\hbar}x}f(p/\hbar)dp, \\ &\quad x\in R,\end{aligned} \tag{B2}$$

and the Fourier transform of the Riesz-Feller derivative of Eq. (3) takes the form

$$F\left\{{}_xD_\theta^\alpha f(x);p/\hbar\right\} = -\psi_\alpha^\theta\left(\frac{p}{\hbar}\right)f\left(\frac{p}{\hbar}\right), \tag{B3}$$

where

$$\psi_\alpha^\theta(k) = |k|^\alpha e^{i[\mathrm{sgn}(k)]\theta\pi/2}, \qquad 0<\alpha\leqslant 2, \quad |\theta|\leqslant\min\{\alpha,2-\alpha\}, \tag{B4}$$

or

$$\psi_\alpha^\theta(p/\hbar) = |p/\hbar|^\alpha e^{i[\mathrm{sgn}(p)]\theta\pi/2}. \tag{B5}$$

Therefore,

$$\begin{aligned}{}_xD_\theta^\alpha f(x) &= -\frac{1}{2\pi}\int_{-\infty}^{\infty}d(p/\hbar)e^{-i\frac{p}{\hbar}x}\psi_\alpha^\theta\left(\frac{p}{\hbar}\right) \times\int_{-\infty}^{\infty}dx'\,e^{i\frac{p}{\hbar}x'}f(x') \\ &= -\frac{1}{2\pi}\int_{-\infty}^{\infty}d(p/\hbar)e^{-i\frac{p}{\hbar}x}|p/\hbar|^\alpha e^{i[\mathrm{sgn}(p)]\theta\pi/2} \times\int_{-\infty}^{\infty}dx'\,e^{i\frac{p}{\hbar}x'}f(x').\end{aligned} \tag{B6}$$

Note that for $\lambda>0$ and using the Fourier transform of $f(x)=\sin(\lambda x)$,

$${}_xD_\theta^\alpha\sin(\lambda x) = -(\lambda)^\alpha\sin\left(\lambda x+\theta\frac{\pi}{2}\right).$$

2. Fractional Riesz-Feller Hamiltonian

The Riesz-Feller hamiltonian was defined in Eq. (10) and is repeated here for conciseness as

$$H_\alpha = -F_\alpha D_\theta^\alpha + V(x), \qquad V(x) = \begin{cases}\infty, & x<0,\\ 0, & 0\leqslant x\leqslant a,\\ \infty, & x>a,\end{cases} \tag{B7}$$

where F_α is the "quantum diffusion constant" with units of [ergs$^{1-\alpha}$ cm$^\alpha$ sec$^{-\alpha}$], and recalling that D_θ^α is the Riesz-Feller derivative defined above. $F_\alpha := -\frac{1}{2}mc^2(\frac{\hbar}{imc})^\alpha$ [27], Eq. (14.11) therein, where m is the "mass" and c is the speed of light.

3. Matrix elements of the fractional Riesz-Feller Hamiltonian

Here we calculate the matrix elements $\langle\lambda_{n'}|H_\alpha|\lambda_n\rangle$ of the fractional Hamiltonian of Eq. (10) [or (B7)], with the basis functions $\langle x|\lambda_n\rangle$ of Eq. (8) [or (A4)]. We use the following identity for the addition of arguments of the sine function,

$$\sin\left(\lambda_n x+\theta\frac{\pi}{2}\right) = \sin(\lambda_n x)\cos\left(\theta\frac{\pi}{2}\right) + \cos(\lambda_n x)\sin\left(\theta\frac{\pi}{2}\right). \tag{B8}$$

Using the above identity [Eq. (B8)], we obtain the following matrix elements of the Riesz-Feller derivative of Eq. (B6),

$$\begin{aligned}\langle\lambda_{n'}|D_\theta^\alpha|\lambda_n\rangle &= \int_0^a dxC\sin(\lambda_{n'}x)\times\left[-C(\lambda_n)^\alpha\sin\left(\lambda_n x+\theta\frac{\pi}{2}\right)\right] \\ &= -(\lambda_n)^\alpha\int_0^a dxC\sin(\lambda_{n'}x)\times\left\{C\sin(\lambda_n x)\cos\left(\theta\frac{\pi}{2}\right)+C\cos(\lambda_n x)\sin\left(\theta\frac{\pi}{2}\right)\right\}\end{aligned}$$

$$= -(\lambda_n)^\alpha \cos\left(\theta\frac{\pi}{2}\right)\langle\,\lambda_{n'}|\lambda_n\rangle - \frac{1}{\hbar}(\lambda_n)^\alpha \sin\left(\theta\frac{\pi}{2}\right) \times \int_0^a dx C\sin(\lambda_{n'}x) C\cos(\lambda_n x)$$

$$= -(\lambda_n)^\alpha \cos\left(\theta\frac{\pi}{2}\right)\langle\,\lambda_{n'}|\lambda_n\rangle - (\lambda_n)^\alpha \sin\left(\theta\frac{\pi}{2}\right) \times C^2 \int_0^a dx \frac{1}{2}[\sin(\lambda_{n'}x+\lambda_n x) + \sin(\lambda_{n'}x-\lambda_n x)]. \quad \text{(B9)}$$

The last term of Eq. (B9) is calculated as follows:

$$C^2\int_0^a dx\frac{1}{2}\times[\sin(\lambda_{n'}x+\lambda_n x)+\sin(\lambda_{n'}x-\lambda_n x)] = \begin{cases} \frac{C^2}{2}\left\{-\frac{\cos[(\lambda_{n'}+\lambda_n)x]}{(\lambda_{n'}+\lambda_n)} - \frac{\cos[(\lambda_{n'}-\lambda_n)x]}{(\lambda_{n'}-\lambda_n)}\right\}_{x=0}^{x=a}, & \lambda_{n'}\neq\lambda_n, \\ \frac{C^2}{2}\left\{-\frac{\cos[(2\lambda_n)x]}{2\lambda_n}\right\}_{x=0}^{x=a}, & \lambda_{n'}=\lambda_n. \end{cases} \quad \text{(B10)}$$

Substituting the limits $x=0$ to $x=a$ one gets

$$C^2\int_0^a dx\tfrac{1}{2}[\sin(\lambda_{n'}x+\lambda_n x)+\sin(\lambda_{n'}x-\lambda_n x)] = \begin{cases} \frac{C^2}{2}\left\{-\frac{\cos[(\lambda_{n'}+\lambda_n)a]}{(\lambda_{n'}+\lambda_n)} - \frac{\cos[(\lambda_{n'}-\lambda_n)a]}{(\lambda_{n'}-\lambda_n)} + \frac{1}{(\lambda_{n'}+\lambda_n)} + \frac{1}{(\lambda_{n'}-\lambda_n)}\right\}, & \lambda_{n'}\neq\lambda_n, \\ \frac{C^2}{2}\left\{-\frac{\cos[(2\lambda_n)a]}{2\lambda_n} + \frac{1}{2\lambda_n}\right\}, & \lambda_{n'}=\lambda_n. \end{cases} \quad \text{(B11)}$$

Therefore, the matrix elements read

$$\langle\lambda_{n'}|D_\theta^\alpha|\lambda_n\rangle = -(\lambda_n)^\alpha\cos\left(\theta\frac{\pi}{2}\right)\langle\lambda_{n'}|\lambda_n\rangle - (\lambda_n)^\alpha\sin\left(\theta\frac{\pi}{2}\right) \times \begin{cases} \frac{C^2}{2}\left\{-\frac{\cos[(\lambda_{n'}+\lambda_n)a]}{(\lambda_{n'}+\lambda_n)} - \frac{\cos[(\lambda_{n'}-\lambda_n)a]}{(\lambda_{n'}-\lambda_n)} + \frac{1}{(\lambda_{n'}+\lambda_n)} + \frac{1}{(\lambda_{n'}-\lambda_n)}\right\}, & \lambda_{n'}\neq\lambda_n, \\ \frac{C^2}{2}\left\{-\frac{\cos[(2\lambda_n)a]}{2\lambda_n} + \frac{1}{2\lambda_n}\right\}, & \lambda_{n'}=\lambda_n. \end{cases} \quad \text{(B12)}$$

Consequently,

$$\langle\lambda_{n'}|H_\alpha|\lambda_n\rangle = F_\alpha(\lambda_n)^\alpha \times \begin{cases} \sin\left(\theta\frac{\pi}{2}\right)\frac{C^2}{2}\left\{-\frac{\cos[(\lambda_{n'}+\lambda_n)a]}{(\lambda_{n'}+\lambda_n)} - \frac{\cos[(\lambda_{n'}-\lambda_n)a]}{(\lambda_{n'}-\lambda_n)} + \frac{1}{(\lambda_{n'}+\lambda_n)} + \frac{1}{(\lambda_{n'}-\lambda_n)}\right\}, & \lambda_{n'}\neq\lambda_n, \\ \cos\left(\theta\frac{\pi}{2}\right) + \sin\left(\theta\frac{\pi}{2}\right)\frac{C^2}{2}\times\left\{-\frac{\cos[(2\lambda_n)a]}{2\lambda_n} + \frac{1}{2\lambda_n}\right\}, & \lambda_{n'}=\lambda_n. \end{cases} \quad \text{(B13)}$$

Limit cases of Eq. (B13):

$$[\langle\lambda_{n'}|H_\alpha|\lambda_n\rangle]_{\alpha=1,\theta=-1} = F_1\lambda_n \begin{cases} -\frac{C^2}{2}\left\{-\frac{\cos[(\lambda_{n'}+\lambda_n)a]}{(\lambda_{n'}+\lambda_n)} - \frac{\cos[(\lambda_{n'}-\lambda_n)a]}{(\lambda_{n'}-\lambda_n)} + \frac{1}{(\lambda_{n'}+\lambda_n)} + \frac{1}{(\lambda_{n'}-\lambda_n)}\right\}, & \lambda_{n'}\neq\lambda_n, \\ -\frac{C^2}{2}\left\{-\frac{\cos[(2\lambda_n)a]}{2\lambda_n} + \frac{1}{2\lambda_n}\right\}, \lambda_{n'}=\lambda_n, \end{cases}$$

where $F_1 = -\frac{\hbar}{2i}c$.

$$[\langle\lambda_{n'}|H_\alpha|\lambda_n\rangle]_{\alpha=2,\theta=0} = \cos(0)F_2\lambda_n^2\delta_{n',n} = \frac{\hbar^2}{2m}\lambda_n^2\delta_{n',n} = \frac{\hbar^2}{2m}\left(\frac{n\pi}{a}\right)^2\delta_{n',n} = \frac{h^2}{8ma^2}n^2\delta_{n',n},$$

where $F_2 = \frac{\hbar^2}{2m}$ and we have substituted the values of the eigenvalues and normalization constant of the basis set functions: $\lambda_n = \frac{n\pi}{a}$ and $C = \frac{\sqrt{2}}{\sqrt{a}}$.

Using these values in Eq. (B13) we arrive at

$$\langle\lambda_{n'}|H_\alpha|\lambda_n\rangle = F_\alpha\left(\frac{n\pi}{a}\right)^\alpha \times \begin{cases} \sin\left(\theta\frac{\pi}{2}\right)\frac{1}{\pi}\times\left\{-\frac{\cos[(n'+n)\pi]}{(n'+n)} - \frac{\cos[(n'-n)\pi]}{(n'-n)} + \frac{1}{(n'+n)} + \frac{1}{(n'-n)}\right\}, & n'\neq n, \\ \cos\left(\theta\frac{\pi}{2}\right) + \sin\left(\theta\frac{\pi}{2}\right)\frac{1}{\pi}\times\left\{-\frac{\cos(2n\pi)}{2n} + \frac{1}{2n}\right\}, & n'=n. \end{cases} \quad \text{(B14)}$$

As $\cos(2n\pi) = 1$ and

$$\cos[(n'+n)\pi] = \begin{cases} 1, & n'+n = \text{even}, \\ -1, & n'+n = \text{odd}, \end{cases}$$

we finally get

$$\langle\lambda_{n'}|H_\alpha|\lambda_n\rangle = B_\alpha(n\pi)^\alpha \times \begin{cases} \sin\left(\theta\frac{\pi}{2}\right)\frac{2}{\pi}\left\{\frac{1}{(n'+n)} + \frac{1}{(n'-n)}\right\}; & n'\neq n, n'+n = \text{odd}; \\ 0; & n'\neq n, n'+n = \text{even}; \\ \cos\left(\theta\frac{\pi}{2}\right); & n'=n; \end{cases} \quad \text{(B15)}$$

where $F_\alpha = -\frac{1}{2}mc^2(\frac{\hbar}{imc})^\alpha$, $B_\alpha = F_\alpha(\frac{1}{a})^\alpha$.

B_α in cgs:

$$\left[\mathrm{g\ cm^2\ s^{-2}}\left(\frac{\mathrm{g\ cm^2\ s^{-1}}}{\mathrm{g\ cm\ s^{-1}}}\right)^{\alpha}\right]\frac{1}{\mathrm{cm}^\alpha} = [\mathrm{g\ cm^2\ s^{-2}(cm)}^\alpha]\frac{1}{\mathrm{cm}^\alpha} = [\mathrm{g\ cm^2\ s^{-2}}] = [\mathrm{ergs}].$$

B_α in atomic units:

$$\left[m_e\mathrm{bohrs}^{2+\alpha}\left(\frac{\hbar}{\mathrm{hartrees}}\right)^{-2}\right]\frac{1}{\mathrm{bohrs}^\alpha} = \left[m_e\mathrm{bohrs}^{2}\left(\frac{\hbar}{\mathrm{hartrees}}\right)^{-2}\right] = [\mathrm{hartrees}].$$

In atomic units $\hbar = 1$, m is expressed in multiples of the electron mass $m_e = 1$, and $c \approx 137$. B_α and $\langle\lambda_{n'}|H_\alpha|\lambda_n\rangle$ are with energy units, so that $\langle\lambda_{n'}|H_\alpha|\lambda_n\rangle/B_\alpha$ is a real nonsymmetric matrix with dimensionless units. We note again that for $\alpha = 2$,

$$\langle\lambda_n|H_2|\lambda_n\rangle = B_2(n\pi)^2 = F_2\left(\frac{1}{a}\right)^2(n\pi)^2 = -\frac{1}{2}mc^2\left(\frac{\hbar}{imc}\right)^2\left(\frac{1}{a}\right)^2(n\pi)^2 = \frac{h^2}{8m}\left(\frac{n}{a}\right)^2, \tag{B16}$$

the well known result of the standard impenetrable one-dimensional rectangular potential well problem; see also Eq. (A3).

[1] O. Svelto, *Principles of Lasers*, 4th ed. (Springer-Verlag, Berlin, 1995).

[2] T. Wimpfheimer, A particle in a box laboratory experiment using everyday compounds, J. Lab. Chem. Educ. **3**, 19 (2015).

[3] H. M. Nussenzveig, The poles of the S-matrix of a rectangular potential well of barrier, Nucl. Phys. **11**, 499 (1959).

[4] R. Zavin and N. Moiseyev, One-dimensional symmetric rectangular well: From bound to resonance via self-orthogonal virtual state, J. Phys. A: Math. Gen. **37**, 4619 (2004).

[5] Y. Luchko, Fractional Schrödinger equation for a particle moving in a potential well, J. Math. Phys. **54**, 012111 (2013).

[6] T. Kato, *Perturbation Theory for Linear Operators* (Springer Science & Business Media, New York, 1966).

[7] N. Moiseyev, *Non-Hermitian Quantum Mechanics* (Springer-Verlag, Berlin, 2011).

[8] W. D. Heiss, Exceptional points of non-Hermitian operators, J. Phys. A: Math. Gen. **37**, 2455 (2004).

[9] W. Chen, Ş. K. Özdemir, G. Zhao, J. Wiersig, and L. Yang, Exceptional points enhance sensing in an optical microcavity, Nature (London) **548**, 192 (2017).

[10] W. D. Heiss, The physics of exceptional points, J. Phys. A: Math. Theor. **45**, 444016 (2012).

[11] C. Dembowski, H.-D. Gräf, H. L. Harney, A. Heine, W. D. Heiss, H. Rehfeld, and A. Richter, Experimental Observation of the Topological Structure of Exceptional Points, Phys. Rev. Lett. **86**, 787 (2001).

[12] J. Doppler, A. A. Mailybaev, B. Julian, U. Kuhl, A. Girschik, F. Libisch, T. J. Milburn, P. Rabl, N. Moiseyev, and S. Rotter, Dynamically encircling an exceptional point for asymmetric mode switching, Nature (London) **537**, 76 (2016).

[13] E. Narevicius, P. Serra, and N. Moiseyev, Critical phenomena associated with self-orthogonality in non-Hermitian quantum mechanics, Europhys. Lett. **62**, 789 (2003).

[14] I. Podlubny, R. L. Magin, and I. Trymorush, Niels Henrik Abel and the birth of fractional calculus, Fractional Calculus and Applied Analysis **20**, 1068 (2017).

[15] N. H. Abel, Oploesning af et par opgaver ved hjelp af bestemte integraler, Magazin for Naturvidenskaberne **2**, 55 (1823); **2**, 205 (1823).

[16] I. Podlubny, R. L. Magin, and I. Trymorush, *Fractional Differential Equations*, Mathematics in Science and Engineering, Vol. 198 (Academic Press, San Diego, 1999).

[17] Y. Luchko and I. Podlubny, FCAA special issue, Fractional Calculus and Applied Analysis **20**, 1053 (2017).

[18] M. M. Meerschaert, B. J. West, and Y. Zhou, Future directions in fractional calculus research and applications, Chaos, Solitons Fractals **102**, 1 (2017).

[19] S. G. Samko, A. A. Kilbas, and O. I. Marichev, *Fractional Integrals and Derivatives: Theory and Applications* (Gordon and Breach Science Publishers, New York and London, 1993).

[20] R. Hilfer, Fractional time evolution, in *Applications of Fractional Calculus in Physics* (World Scientific, Singapore, 2000), pp. 87–130.

[21] F. Mainardi, Y. Luchko, and G. Pagnini, The fundamental solution of the space-time fractional diffusion equation, Fractional Calculus and Applied Analysis **4**, 153 (2001).

[22] H. Takayasu, *Fractals in the Physical Sciences, Nonlinear Science: Theory and Applications* (Manchester University Press, Manchester, New York, 1989).

[23] N. Laskin, Fractional Schrödinger equation, Phys. Rev. E **66**, 056108 (2002).

[24] K. Sayevand and K. Pichaghchi, Reanalysis of an open problem associated with the fractional Schrödinger equation, Theor. Math. Phys. **192**, 1028 (2017).

[25] S. Bayin, Definition of the Riesz derivative and its application to space fractional quantum mechanics, J. Math. Phys. **57**, 123501 (2016).

[26] M. Jeng, S.-L.-Y. Xu, E. Hawkins, and J. M. Schwarz, On the nonlocality of the fractional Schrödinger equation, J. Math. Phys. **51**, 062102 (2010).

[27] R. Herrmann, *Fractional Calculus: An Introduction for Physicists*, 2nd ed. (World Scientific Publishing, Singapore, 2014).

[28] O. Defterli, M. D'Elia, Q. Du, M. Gunzburger, R. Lehoucq, and M. M. Meerschaert, Fractional diffusion on bounded domains, Fractional Calculus and Applied Analysis **18**, 342 (2015).

[29] B. Baeumer, M. Kovács, M. M. Meerschaert, and H. Sankaranarayanan, Boundary conditions for fractional diffusion, J. Comput. Appl. Math. **336**, 408 (2018).

[30] B. Al-Saqabi, L. Boyadjiev, and Yu. Luchko, Comments on employing the Riesz-Feller derivative in the Schrödinger equation, Eur. Phys. J.: Spec. Top. **222**, 1779 (2013).

[31] C. M. Bender, Making sense of non-Hermitian Hamiltonians, Rep. Prog. Phys. **70**, 947 (2007).

[32] R. El-Ganainy, K. G. Makris, M. Khajavikhan, Z. H. Musslimani, S. Rotter, and D. N. Christodoulides, Non-Hermitian physics and PT symmetry, Nat. Phys. **14**, 11 (2007).

[33] L. Lu and X. Yu, The fractional dynamics of quantum systems, Ann. Phys. **392**, 260 (2018).

[34] R. P. Feynman, Space-time approach to non-relativistic quantum mechanics, Rev. Mod. Phys. **20**, 367 (1948).

[35] A. Kossakowski, On quantum statistical mechanics of non-Hamiltonian systems, Rep. Math. Phys. **3**, 247 (1972).

[36] G. Lindblad, On the generators of quantum dynamical semigroups, Commun. Math. Phys. **48**, 119 (1976).

[37] V. Gorini, A. Kossakowski, and E. C. G. Sudarshan, Completely positive dynamical semigroups of N-level systems, J. Math. Phys. **17**, 821 (1976).